

Exploration of Human Serum Lipoprotein Supramolecular Phospholipids Using Statistical Heterospectroscopy in n -Dimensions (SHY- n): Identification of Potential Cardiovascular Risk Biomarkers Related to SARS-CoV-2 Infection

Reika Masuda,[◆] Samantha Lodge,[◆] Luke Whiley, Nicola Gray, Nathan Lawler, Philipp Nitschke, Sze-How Bong, Torben Kimhofer, Ruey Leng Loo, Berin Boughton, Annie X. Zeng, Drew Hall, Hartmut Schaefer, Manfred Spraul, Girish Dwivedi, Bu B. Yeap, Tammo Diercks, Ganeko Bernardo-Seisdedos, José M. Mato, John C. Lindon, Elaine Holmes,* Oscar Millet,* Julien Wist,* and Jeremy K. Nicholson*



Cite This: *Anal. Chem.* 2022, 94, 4426–4436



Read Online

ACCESS |



Metrics & More

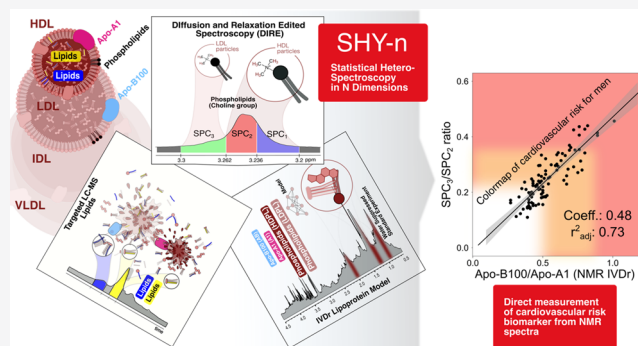


Article Recommendations



Supporting Information

ABSTRACT: SARS-CoV-2 infection causes a significant reduction in lipoprotein-bound serum phospholipids give rise to supramolecular phospholipid composite (SPC) signals observed in diffusion and relaxation edited ^1H NMR spectra. To characterize the chemical structural components and compartmental location of SPC and to understand further its possible diagnostic properties, we applied a Statistical Heterospectroscopy in n -dimensions (SHY- n) approach. This involved statistically linking a series of orthogonal measurements made on the same samples, using independent analytical techniques and instruments, to identify the major individual phospholipid components giving rise to the SPC signals. Thus, an integrated model for SARS-CoV-2 positive and control adults is presented that relates three identified diagnostic subregions of the SPC signal envelope (SPC_1 , SPC_2 , and SPC_3) generated using diffusion and relaxation edited (DIRE) NMR spectroscopy to lipoprotein and lipid measurements obtained by in vitro diagnostic NMR spectroscopy and ultrahigh-performance liquid chromatography–tandem mass spectrometry (UHPLC–MS/MS). The SPC signals were then correlated sequentially with (a) total phospholipids in lipoprotein subfractions; (b) apolipoproteins B100, A1, and A2 in different lipoproteins and subcompartments; and (c) MS-measured total serum phosphatidylcholines present in the NMR detection range (i.e., PCs: 16.0,18.2; 18.0,18.1; 18.2,18.2; 16.0,18.1; 16.0,20.4; 18.0,18.2; 18.1,18.2), lysophosphatidylcholines (LPCs: 16.0 and 18.2), and sphingomyelin (SM 22.1). The $\text{SPC}_3/\text{SPC}_2$ ratio correlated strongly ($r = 0.86$) with the apolipoprotein B100/A1 ratio, a well-established marker of cardiovascular disease risk that is markedly elevated during acute SARS-CoV-2 infection. These data indicate the considerable potential of using a serum SPC measurement as a metric of cardiovascular risk based on a single NMR experiment. This is of specific interest in relation to understanding the potential for increased cardiovascular risk in COVID-19 patients and risk persistence in post-acute COVID-19 syndrome (PACS).



INTRODUCTION

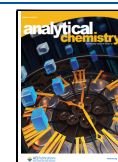
SARS-CoV-2 infection causes a complex range of immunologically driven systemic effects in multiple organ systems, and this manifests as multiple biochemical pathway disruptions.^{1,2} Some of these abnormalities are dependent on the severity of the disease in the acute phase and may show long-term persistence associated with PACS.³ In addition to the cytokine panel proposed as an early indicator of individuals likely to develop PACS,⁴ we previously advocated using metabolic markers as indicators of phenotypic recovery (phenoreversion) associated with disease remission.^{5,6} Metabolic markers can be

derived from mass spectrometry (MS) or NMR spectroscopy measurements of biofluids such as plasma to give a broad palette of functional windows with which to assess recovery. COVID-19 has multiple associated pathologies including

Received: December 13, 2021

Accepted: February 18, 2022

Published: March 1, 2022



cardiovascular and neurological diseases,^{7,8} and there is much interest in assessing how long-term disease risks might also change for people who have been afflicted by COVID-19 and PACS and in the development of new metrics for assessment.

High-resolution ¹H NMR spectroscopy has long been used to study the biochemical composition and variation of blood serum in health and disease.^{9–13} Multiple methods involving both physical NMR experiments and statistical spectroscopic approaches^{6,7} have been applied to recover information on the complex heterogeneous and multicompartmental components (metabolites,^{14,15} glycoproteins,^{16,17} and lipoproteins^{11,18–20}) in plasma or serum. A key analytical advantage provided by NMR spectroscopy is the ability to study supramolecular assemblies such as lipoproteins in blood plasma or serum nondestructively using a variety of spectral editing techniques to attenuate broad macromolecular NMR signal envelopes.²¹ Additionally, translational diffusion editing can also be employed using pulsed-field gradients^{22,23} for the selective attenuation of signals from small molecules that diffuse rapidly in solution. Motional editing in two-dimensional experiments^{24–26} can also be combined with T₂ relaxation as in diffusion and relaxation editing^{27,28} (DIRE) ¹H NMR spectroscopy. DIRE enhances signals from molecules that exhibit slow translational diffusion rates that also have a high level of local segmental motion. DIRE NMR experiments when applied to the plasma of SARS-CoV-2 positive and negative and control patients revealed a strong diagnostic pattern involving lipoprotein-bound phospholipid and glycoprotein signals.²⁸ Additionally, we and others have shown that NMR-generated lipoprotein signals are profoundly altered in SARS-CoV-2 infection^{28–32} and that some of these lipoproteins give further information on cardiovascular disease risk factors that can then be statistically linked to novel disease biomarkers.

A range of statistical spectroscopic methods have been shown to be powerful for metabolite identification,³³ structure elucidation, pathway connectivity, and compartmental analysis. Both Statistical T_{OT}al Correlation Spectroscopy (STOCSY³⁴) and Statistical Heterospectroscopy (SHY³⁵) approaches are complementary to the conventional NMR structure assignment and have the advantage of being able to statistically link structural and chemical components that have been measured in parallel using different spectroscopic experiments.³⁶ We previously applied STOCSY methods to observe the relationships of the differential diagnostic cluster of lipoprotein-related ⁻¹N-(CH₃)₃ headgroup signals from phospholipids that we designated as a supramolecular phospholipid composite signal or SPC (observable in DIRE spectra), which was diagnostic in SARS-CoV-2 infection.²⁸ The SPC signal shows considerable underlying complexity,³⁷ and here, we have used an extended range of statistical spectroscopic tools and complementary serum mass spectrometry for both control and SARS-CoV-2 positive patients to probe the signal for the SPC complex in terms of molecular composition and compartmentation. Thus, for the same serum samples, we integrated and correlated both the paired SPC signal data with phospholipidomic data³⁸ and in vitro diagnostic lipoprotein data with quantified phospholipid subfraction data and apolipoprotein B100, A1, and A2 data.³⁹ In this way, we were able to strengthen our understanding of the location, composition, and potential diagnostic value of the SPC peaks, particularly in relation to cardiovascular disease risk, both in general and in COVID-19 related cardiovascular complications.

MATERIALS AND METHODS

Patient Enrollment and Sample Collection. Blood serum samples were collected from adult individuals in a study initiated at CIC bioGUNE. Healthy control serum samples were collected under equivalent conditions before the COVID-19 pandemic. The cohort consisted of control participants (*n* = 99) and participants who tested positive for SARS-CoV-2 infection from RT–PCR on nasopharyngeal swab samples (*n* = 32), collected at the Cruces University Hospital (Barakaldo, Spain). All of the information available about the cohort demographics is summarized in Table S1. Serum samples were collected by the Basque Biobank for Research (BIOEF), in which participants provided informed consent to clinical investigations, according to the Declaration of Helsinki, and data were anonymized to protect participant confidentiality. The sample-handling protocol was evaluated and approved by the Comité de Ética de Investigación con medicamentos de Euskadi (CEIm-E, PI+CES-BIOEF 2020-04 and PI219130). The shipment of human samples to the Australian National Phenome Centre (ANPC) had the approval of the Ministry of Health of the Spanish Government. Samples were stored at -80 °C upon receipt at the Australian National Phenome Center (ANPC). Samples were imported under Import Permit 0004275122 issued by the Australian Government Department of Agriculture, Water and the Environment. Research was conducted in accordance with the Murdoch University Human Ethics Committee approval (no. 2020/052 and 2020/053).

Materials. SampleJet NMR tubes of 5 mm outer diameter, POM balls for sealing the tube caps, and phosphate buffer (75 mM Na₂HPO₄, 2 mM NaN₃, and 4.6 mM sodium trimethylsilyl propionate-[2,2,3,3-2H₄] (TSP) in H₂O/D₂O 4:1, pH 7.4 ± 0.1) were purchased from Bruker.

NMR Sample Preparation. Serum samples were thawed at 20 °C for 30 min and then centrifuged at 13,000g for 10 min at 4 °C. Samples were prepared in 5 mm outer diameter SampleJet NMR tubes, following the recommended procedures for in vitro analytical and diagnostics procedures²⁰ using 300 μL of serum mixed with 300 μL of phosphate buffer. NMR SampleJet tubes were sealed with POM balls added to the caps. Processing procedures were compliant with our previous recommendations on sample handling and storage for COVID-19 samples.⁴⁰

600 MHz Proton NMR Spectroscopy and In Vitro Diagnostic Experiments. NMR spectroscopic analyses were performed on a 600 MHz Bruker Avance III HD spectrometer equipped with a 5 mm BBI probe and fitted with the Bruker SampleJet robotic cooling system set to 5 °C. A full quantitative calibration was completed before the analysis using a previously described protocol.²⁰ For each sample a single one-dimensional (1D) NMR experiment was performed using the Bruker In Vitro Diagnostics research (IVDr) methods, and the standard 1D experiment was performed with solvent presaturation (32 scans, 98k data points, spectral width of 30 ppm, and experiment time of 4 min). Regression experiments were performed to quantify 112 parameters of main serum lipoprotein classes and subclasses using the Bruker IVDr Lipoprotein Subclass Analysis (B.I.LISA) method.³⁹ This was completed by quantifying the $-CH_2$ ($\delta = 1.25$) and $-CH_3$ ($\delta = 0.8$) peaks of the 1D spectrum after normalization to the Bruker QuantRef manager within Topspin using a PLS-2 regression model. The lipoprotein subclasses included different molecular components of very low-density lipoprotein (VLDL,

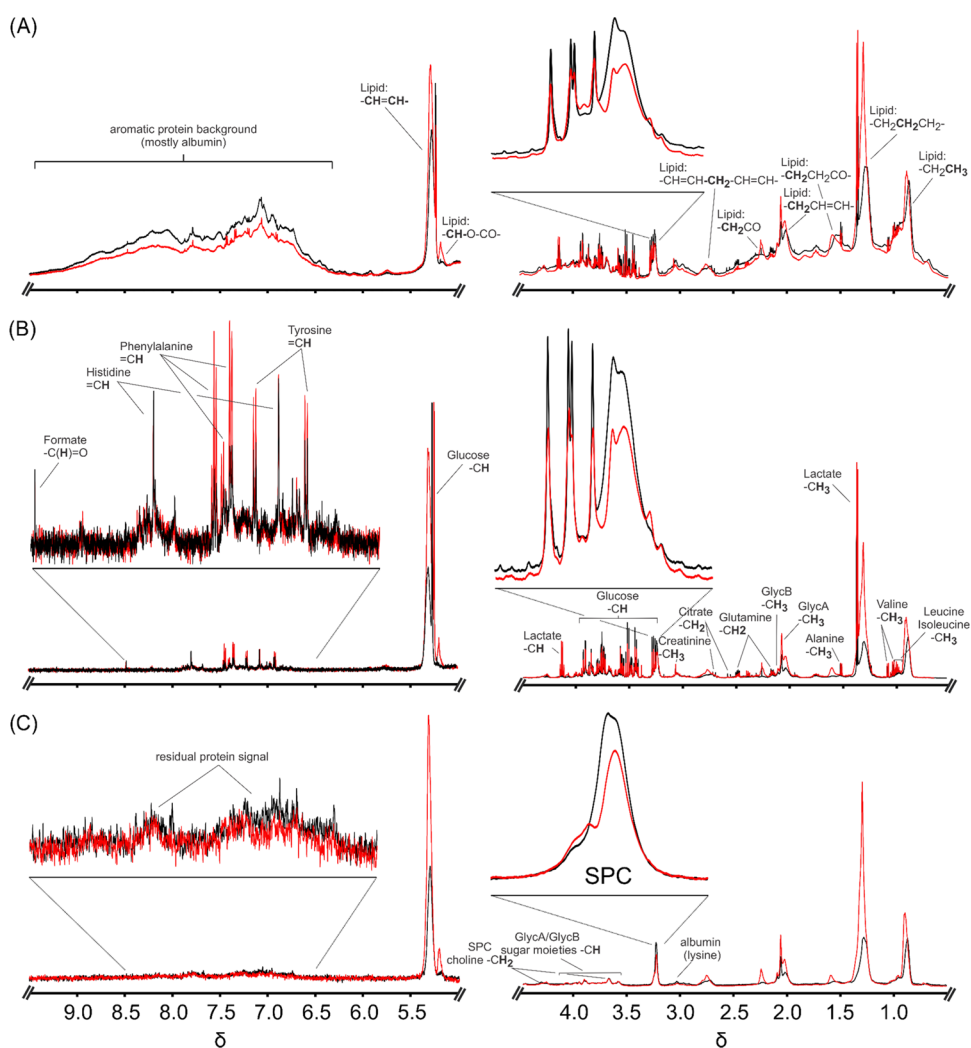


Figure 1. NMR spectra of representative serum samples. (A–C) The standard 600 MHz 1D water-suppressed NMR spectrum, the water-suppressed CPMG spin-echo NMR spectrum, and the DIRE NMR spectrum of normal human blood serum for a healthy (black trace) and SARS-CoV-2 infected (red trace) patient, respectively. The spectra are typical, showing a broad envelope of proton resonances from lipoproteins and proteins (A), a series of well-resolved signals from small molecules (B), and well-resolved signals from slow-diffusing species with a high degree of local segmental motion resulting from combined diffusion and T_2 relaxation editing (C). Expansions of the $-\text{N}-\text{CH}_3$ region for each are also shown with the complex overlapped SPC peaks being clear in (C). The SPC peak has been partially assigned in previous studies and was thought to have both HDL and LDL phospholipid components.^{37,43,44}

0.950–1.006 kg/L), low-density lipoprotein (LDL, density 1.09–1.63 kg/L), intermediate-density lipoprotein (IDL, density 1.006–1.019 kg/L), and high-density lipoprotein (HDL, density 1.063–1.210 kg/L). The LDL subfraction was further divided into six density classes (LDL1, 1.019–1.031 kg/L; LDL2, 1.031–1.034 kg/L; LDL3, 1.034–1.037 kg/L; LDL4, 1.037–1.040 kg/L; LDL5, 1.040–1.044 kg/L; and LDL6, 1.044–1.063 kg/L), and the HDL subfractions were placed in four different density classes (HDL1, 1.063–1.100 kg/L; HDL2, 1.100–1.125 kg/L; HDL3, 1.125–1.175 kg/L; and HDL4, 1.175–1.210 kg/L). Table S2 contains a full description of the lipoprotein parameters.

Diffusion and Relaxation Editing (DIRE) NMR Spectroscopy. Upon completion of the standard 1D experiment with solvent presaturation, the DIRE experiment was run with 64 scans, 98k data points, a spectral width of 30 ppm, and with a total experiment time of 4 min 25 s per sample.²⁸

Data Preprocessing and Statistical Evaluation. All data points of the standard 1D spectrum with water suppression

and DIRE spectra were corrected for quantification to account for variability within the instrument, and the 1D spectrum was calibrated to the α anomeric proton signal of glucose at δ 5.23. The DIRE spectrum was baseline corrected using an asymmetric least-squares routine; spectral regions containing the residual water peak (δ 4.50–4.90) and regions containing predominantly noise ($\delta < 0.4$ and $\delta > 9.5$) were excluded from the analyses. To obtain signal estimates of the SPC peaks spectral intensities of the regions, SPC₁ δ 3.20–3.236; SPC₂ δ 3.236–3.262; and SPC₃ δ 3.262–3.30, were integrated from the DIRE spectra after preprocessing. The Spearman's correlation coefficient (r) for these three integrals amounted to values ranging between 0.6 and 1.

LC-MS/MS Lipid Analysis. Lipid analysis was performed by ultrahigh-performance liquid chromatography–tandem mass spectrometry (UHPLC–MS/MS) according to previously established data acquisition, processing, and analysis workflows.³⁸ Serum samples were thawed, and 10 μL aliquots were placed into a 96-well plate, to which 90 μL of extraction

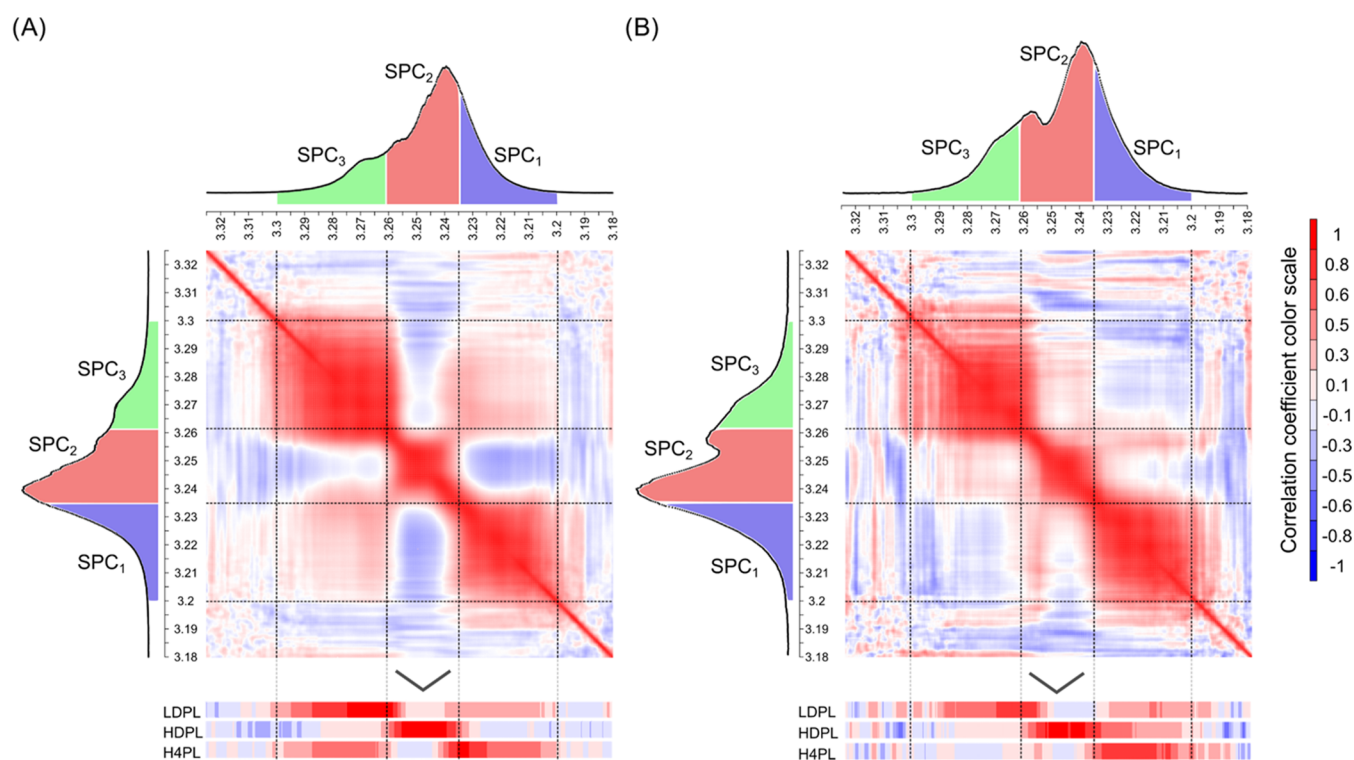


Figure 2. The internal correlation structure of the SPC peak complex: Autocorrelation (STOCSY) heatmaps of the SPC spectral region using DIRE NMR experiments and selected serum lipid components. Three distinct SPC spectral high-correlation regions are observed with chemical shift boundaries optimized using Spearman's r_s (range 0.6–1.0). (A) Controls and (B) SARS-CoV-2 infected patients. Lower panels show correlations of SPC signals with lipoprotein phospholipid components derived from the IVDr measurements on the same samples: H4PL (SPC₁), HDPL (SPC₂), and LDPL (SPC₃). SPC₁ and SPC₂ are mainly from HDL phospholipids, and SPC₃ is from LDL phospholipids.

solvent (propan-2-ol) containing stable-isotope-labeled internal standards (Lipidizer™ Internal Standard Kit from Sciex (Framingham, MA), SPLASH(R) LIPIDOMIX(R), Lyso PI 17:1, Lyso PG 17:1, and Lyso PS 17:1 (Avanti Polar Lipids, Alabaster, AL)) was added. Samples were shaken for 10 min and chilled at $-20\text{ }^{\circ}\text{C}$ for 20 min before centrifugation at $3900g$ for 15 min at $4\text{ }^{\circ}\text{C}$. The resulting supernatants were transferred to a 96-well plate and placed in an autosampler chilled to $10\text{ }^{\circ}\text{C}$ for analysis. Pooled reference serum samples were analyzed as quality control (QC) samples to monitor analytical performance, prepared as per study samples and injected following every 10th sample injection. Peak picking and data normalization were conducted using SkylineMS⁴¹ and in-house-developed R scripts. Concentrations were calculated using stable-isotope-labeled internal standards. Analytes were excluded if the relative standard deviation exceeded 30% in the quality control samples. Signal drift was accounted for using random forest signal correction (QC-RFSC) from the statTarget R library.⁴²

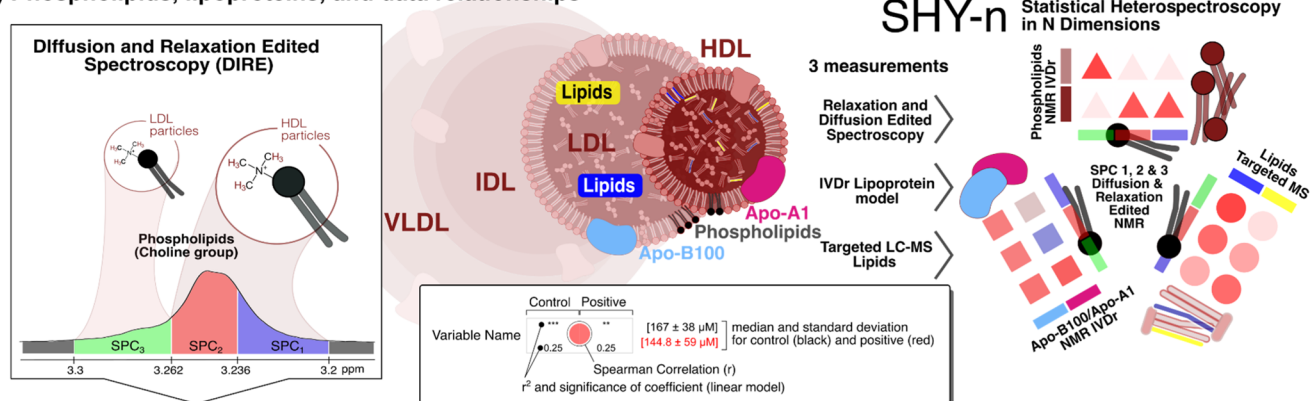
Statistical HeterospectroscopyY (SHY) Analysis. To understand further information carried in the SPC peaks, we have applied the SHY experimental concept³⁵ to integrating orthogonal spectroscopic data sets captured for identical samples and extended this to n -spectroscopic dimensions (SHY- n). In this case, we included SPC intensity data for the DIRE spectra (the first dimension), lipoprotein phospholipid concentration and compartment information in the second virtual dimension (SHY-1 experiment), lipoprotein biological risk biomarker information in the third virtual dimension (SHY-2 experiment), and MS-generated phospholipid data in the fourth virtual dimension (SHY-3 experiment).

RESULTS AND DISCUSSION

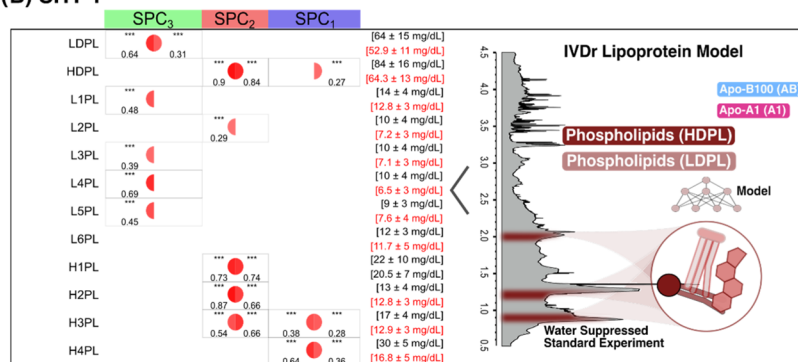
NMR Spectroscopy of Serum. The first aim of this work was to uncover the chemical and compartmental nature of the previously identified “SPC” signal and to further understand its possible diagnostic properties. Here, the multicomponent SPC peak is generated from the DIRE NMR experiment as described previously²⁸ and is the residual intensity in a combined relaxational and translational diffusion editing experiment. We related the SPC intensity variation to metrics obtained from different NMR experiments performed with the same serum samples. Thus, a number of data sets generated from the same sample set were statistically linked to the DIRE-generated SPC peak using SHY.³⁵ Experimental details of all NMR spectroscopic experiments including DIRE are detailed in Figures 1 and S1, whereas Figure 1A,B describes the lipoprotein signature and most common small-molecule peaks together with the glycoprotein acetyl peaks at δ 2.03 and δ 2.07, which are commonly referred to as GlycA and GlycB in the literature. The DIRE spectra in Figure 1C highlight the methylene groups of the choline moiety connected to the $-^+\text{NMe}_3$ residue of SPC and some ring protons of *N*-acetylglucosamine and *N*-acetylneuraminic acid, which are associated with GlycA and GlycB. These additional features are usually not detected in a conventional single pulse or CPMG experiment due to signal overlap.

Interrogating the SPC NMR Signal Complex in Intact Serum. Previous work indicated that the SPC complex signal represented more than one phospholipid species in several magnetic (compartmental) environments.^{28,37,44} To understand the distribution of the information content across the SPC peak complex, we first calculated the two-dimensional

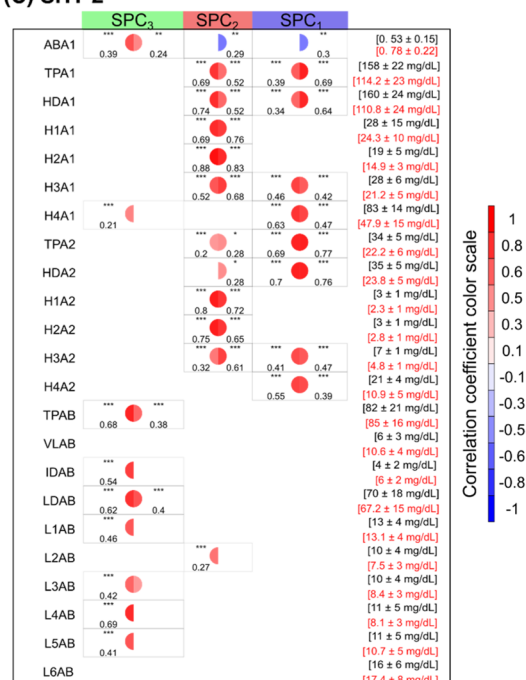
(A) Phospholipids, lipoproteins, and data relationships



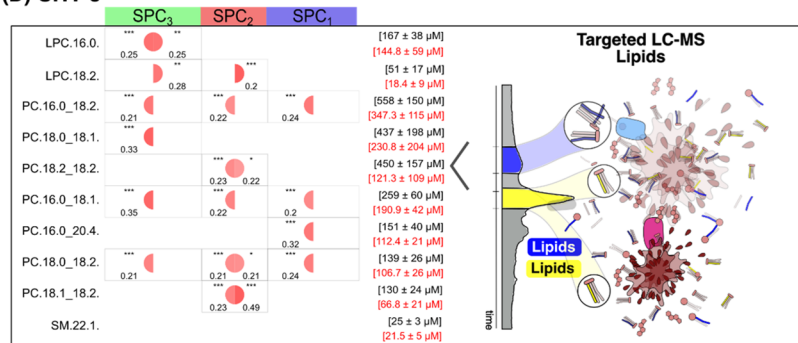
(B) SHY-1



(C) SHY-2



(D) SHY-3



Key (prefix): VL = VLDL, ID = IDL, LD = LDL, HD = HDL, L1-L6 = LDL subfractions, H1-H4 = HDL subfractions, TP = total particle number, AB = Apo-B100
 Key (suffix): PL = Phospholipids, A1 = apolipoprotein-A1, AB = apolipoprotein-B100 (ABA1 = Apo-B100/Apo-A1 ratio)
 Absence of a half-SHY marker indicates no significant correlation

Figure 3. Overview of the Statistical Heterospectroscopy in n -dimensions (SHY- n) approach to interrogating the SPC NMR signal complex. The SHY- n method serially correlates (A) the segments of the composite SPC peak, SPC₁, SPC₂, and SPC₃ with (B) phospholipids (SHY-1), (C) apolipoproteins A1 and B100 (SHY-2) modeled from standard water-suppressed NMR spectra,²⁰ and (D) lipids measured by targeted liquid chromatography–mass spectrometry (LC–MS) (SHY-3). Each cell is divided in half as explained in the inset, to display the results for control (left) and SARS-CoV-2 positive people (right). The color code describes the Spearman correlation coefficient that ranges from negative (blue = anticorrelation) to positive (red = correlation) values. Only significant correlations are shown. For each variable (row), the mean and standard deviation are displayed on the right-hand side, both for control and infected (acute phase) participants. On the top, an infographic illustrates the lipoprotein fractions and their constituents. Special colors associate compounds with the measurement that quantifies them: the choline group of phospholipids (black) with diffusion and relaxation edited (DIRE) NMR experiment, lipids (yellow and dark blue) with targeted LC–MS, and phospholipids fractions and the apolipoprotein A1 (pink) and B100 (light blue) with the NMR IVDr method.

STOCSY (autocorrelation) plot for the region of interest (δ 3.2–3.3), and these plots are shown for control and SARS-CoV-2 infected patients in Figure 2A,B, respectively. Despite the different spectral profiles and intensities, the signals for SARS-CoV-2 patients being weaker than those from controls, we observed that the autocorrelation signatures are similar with three distinct regions of autocorrelation with median Spearman's correlation coefficient (r_s) values in the range of 0.6–1

(Figure 2). We had previously suggested more simplistically that these peaks correspond to HDL and LDL fractions as SPC-A and SPC-B, respectively.^{28,37,44} But further investigation of the internal correlations between the SPC signal envelope reveals more complexity. The correlation map with the IVDr-generated lipoprotein phospholipid components shows further lipoprotein subfraction definition by density as follows: HDL4 (SPC₁ δ 3.20–3.236); HDL1, 2, and 3 (SPC₂ δ

3.236–3.262); and LDL total phospholipids (SPC₃ δ 3.262–3.30). A more detailed correlation of the SPC peaks in relation to other lipoprotein compartments is also shown in Figure 3.

The high correlation of chemical shift variables that following the main diagonal of the correlation matrix indicates three signal cluster groups for SPC carry the same statistical information and thus can be integrated as three individual SPC regions for further statistical analysis. It is worth noting that the three SPC regions do not necessarily align with peak apexes present in each individual trace because of the differential overlap of the embedded signals (see Figure S1a and b). A statistical heterospectroscopic analysis in relation to the lipoprotein phospholipids enabled annotation of the peaks as described above. The designations SPC₁, SPC₂, and SPC₃ supersede our previous annotation of “SPC-A” and “SPC-B”,²⁸ which were based on the centroids of the chemical shifts of the main fractions visible to NMR, HDL and LDL, rather than their spectroscopic information contents across the SPC chemical shift regions.^{37,44}

Statistical Heterospectroscopy of SPC Peaks in *n*-Dimensions (SHY-*n*). The approach to heterospectroscopic statistical correlation is illustrated further in Figure 3A, which shows the integrated SPC₁, SPC₂, and SPC₃ regions in relation to other orthogonally measured data sets of the same sample. A structural comparison of the major lipoproteins in relation to their phospholipid and apolipoprotein locations is presented in Figure 3A. The relationships between the various SHY-*n* dimensions for NMR and MS together with a key for interpreting the various SHY-*n* submaps are also shown in Figure 3A.

Analysis of the SPC signals in Relation to Lipoprotein Phospholipids (SHY-1). The first level of the SHY experiment (SHY-1) is generated from the IVDr NMR data on the phospholipid-containing compartments in LDL and HDL subfractions with both structural and compartmental contributions (Figure 3B). Full IVDr measurements on each serum sample were made using Bruker B.I.LISA software, and all data are tabulated in Table S2. We extracted the individual values for each of the lipoprotein phospholipid compartments from this set and correlated those with the SPC integrals. The correlation coefficients between the integrated SPC regions and each lipoprotein phospholipids were color-coded and split to show the controls (left half of the semicircle) and the SARS-CoV-2 patients (right half of the semicircle) in what we term a “Half-SHY” plot within the 2D SHY array (DIRE NMR to lipoprotein phospholipids). The numerical values of the coefficients of determination of a linear model, adjusted r^2 , for each relationship are also displayed. High correlations were observed for SPC₃ and the total phospholipid fraction in the main LDL lipoprotein class (LDPL), and SPC₂ and the total phospholipid fraction in HDL (HDPL) (Figures 2 and 3B). Previously published reports^{19,37,44,45} and further experimental evidence²⁸ confirming our previous findings support that SPC₃ and SPC₂ stem from the LDL and HDL phospholipid choline headgroups. The strong correlation between H3PL and H4PL (phospholipids in the HDL subfractions 3 and 4) and SPC₁ is consistent with prior observations of shifts toward lower frequencies of protons in the choline headgroup as the density of the lipoprotein increases.^{28,37,45}

The Half-SHY plots are found to be similar for both control and infected patients, as shown in Figure 3B, which is expected in this SHY dimension as the two techniques are measuring the same compounds. Discrepancies are explained by the fact that

only three statistical regions are considered for SPC, although each region stems from several broad and overlapped contributions of lipoprotein subfractions. In controls, SPC₃ is dominated by LDL phospholipids (particularly in LDL1, 3, 4, and 5 with high adjusted r^2 values) and a smaller contribution from HDL4. The LDL contributions to SPC₃ are lowered in SARS-CoV-2 positive individuals.^{28,46,47} SPC₂ is dominated by HDL contributions (HDL subfractions 1–3) in both control and SARS-CoV-2 patients with an additional contribution from LDL1, LDL2, and LDL3 subfractions, but the absolute levels of HDL phospholipids are reduced in SARS-CoV-2 infection (Figure S5). SPC₁ is dominated by HDL3 and HDL4 phospholipid components, and these are of interest because the small high-density lipoproteins that are depleted in SARS-CoV-2 infection also contain high levels of fibrinolytic proteins^{48,49} that may be related to the significant thrombosis/clotting disorder associated with this disease, as previously reported,^{50,51} and therefore, HDL4, SPC₃, and SPC₁ might also carry information on blood clotting events (although this remains to be investigated).

SPC Correlations with Cardiovascular Apolipoprotein Risk Markers (SHY-2). The second level of SHY applied here also exemplifies the power of statistical correlation as it allows the association of different compounds that are in the same biological compartment. IVDr methods predict serum concentrations of multiple apolipoproteins that are cardiovascular risk markers, based on previous assumptions about their presence in lipoproteins.^{52,53} We note that the SPC regions are highly correlated with several of these components through their compartmental sharing connectivity that is revealed in another dimension of the SHY-*n* matrix (SHY-2, Figures 3C and S6). This has no chemical NMR contribution because the apolipoproteins A1 and B100 do not contain choline moieties, but they share a common compartment with the phospholipids. We note that SARS-CoV-2 infection has relatively little influence on the distribution of the connectivity to the various SPC components. The serum ApoB100/A1 ratio is a well-established marker of cardiovascular,⁵⁴ atherosclerosis,^{55,56,58} and myocardial infarction risks.^{54,57} We have previously shown that SARS-CoV-2 infection is associated with a reduction in ApoA1 but with no significant changes to ApoB100.²⁸ The ApoB100 is mainly associated with the LDL component, and the ApoA2 in HDL1 and HDL2 mainly correlates with the SPC₂ region intensity, whereas the ApoA2 in HDL3 and HDL4 mainly correlates with SPC₁ (Figure 3C). There appears to be little direct diagnostic value in ApoA2 with respect to SARS-CoV-2 infection, so it is not considered further here, although we note that ApoA2 is an important marker in many other diseases including diabetes and cancers so the SPC₂ NMR region may have further diagnostic value that remains to be investigated.

The SPC₃ regions (particularly LDL subfractions 3, 4, and 5 (Figure 3C)) are highly correlated with the total ApoB100/A1 ratio (ABA1) in controls and to a lesser extent, but still highly significant, in the infected patients. The SPC₃/SPC₂ ratio correlates with the ABA1 ratio and so appears to be a new surrogate marker for cardiovascular risk. The high level of cardiovascular risks in COVID-19 patients is well documented^{59–61} and echoes the increased presentation of myocardial infarction following the outbreak of the first SARS virus in 2003.⁶² Notably, the SPC₂ region is strongly anticorrelated to the ABA1 level (Figure 3C). In general, SPC₃ correlates strongly with the apolipoprotein B100, while SPC₂

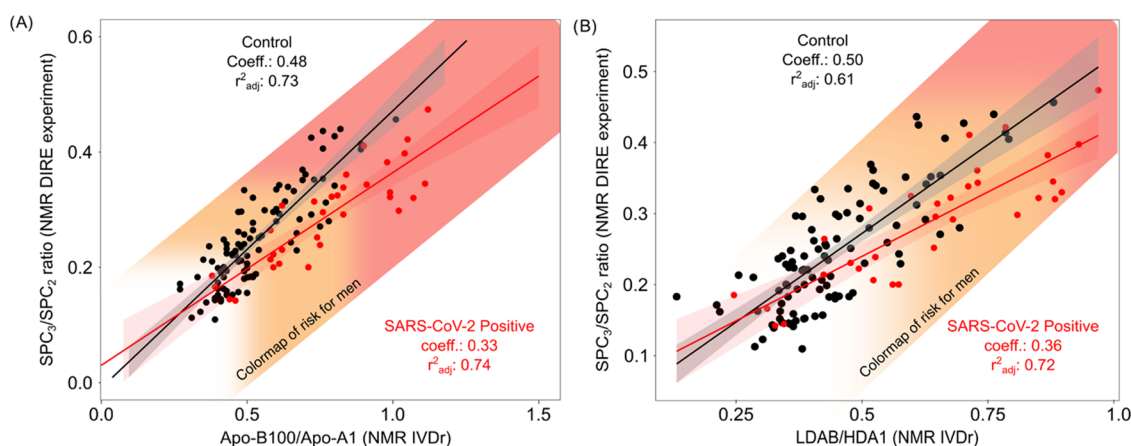


Figure 4. Relationships between SPC signal intensities and cardiovascular disease risk markers: (A) Regression of the DIRE-derived SPC_3/SPC_2 ratio against the apolipoprotein B100/A1 ratio for control (black) and SARS-CoV-2 positive (red) individuals. (B) Regression of the DIRE-derived SPC_3/SPC_2 ratio against the apolipoprotein B100 in LDL/A1 in the HDL ratio for control (black) and SARS-CoV-2 positive (red) individuals. (A) SPC_3/SPC_2 ratio for the whole data set was regressed against the ApoB100/ApoA1 ratio, a dummy variable for groups and the interaction of the two regressors. The significance of the latter (2.16×10^{-3}) indicates that the ratio is affected differently for both groups. Consequently, the two groups were modeled separately yielding a higher coefficient for the control group (coeff.: 0.48) than for the SARS-Cov-2 positive group (coeff.: 0.33). (B) The SPC_3/SPC_2 ratio for the whole data set was regressed against the ApoB100 in LDL/ApoA1 in HDL, a dummy variable for groups and the interaction of the two regressors. The significance of the latter (2.46×10^{-2}) indicates that the ratio is affected differently for both groups. Consequently, the two groups were modeled separately yielding a higher coefficient for the control group (coeff.: 0.50) than for the SARS-CoV-2 positive group (coeff.: 0.36). A colormap representing the cardiovascular risk for men based on ABA1 according to the work of Walldius et al.^{54,65,66} is shown in the background. In men, the apolipoprotein B100/A1 ratio of 0.4–0.7 is considered as low risk, 0.7 to 0.9 as medium risk, and 0.9 and higher as high risk of developing cardiovascular disease. Although several individuals in the control group are found in the red “at risk” region, this number was higher in the infected group.

correlates strongly with ApoA1 parameters. Consequently, there is a strong correlation/anticorrelation pattern between the ApoB100/ApoA1 ratio (ABA1) and SPC_3 and SPC_2 , respectively (or with LDAB/HDA1 in Figure 4B). As SHY-2 already confirmed that SPC_3 stems from the LDL subfraction that is known to carry exactly one unit of ApoB100 per particle, the first correlation is expected.⁵⁴ The anticorrelation between ABA1 and SPC_2 was not expected. It is also worth noting that this anticorrelation is a rare case where the association is stronger for the infected group than the controls. There are multiple strong correlations between SPC_2 and the apolipoproteins in control and SARS-CoV-2 infected individuals.

Serum apolipoprotein A1, which transports lipids out of endothelial cells,⁶³ is particularly reduced in COVID-19 (Figure 3C).⁶⁴ SPC_2 is highly correlated with ApoA1 in HDL fractions 1–3 and SPC_1 to ApoA1 in H4, so SPC_2 can also be hypothesized to be a valuable cardiovascular risk marker. To test this further, we plotted the SPC_3/SPC_2 ratio against the ApoB100/ApoA1 ratio for both healthy controls and SARS-CoV-2 positive individuals and found them to be highly correlated ($r = 0.85$ and 0.86), respectively, with $p = 2.2 \times 10^{-16}$ and 1.67×10^{-9} , respectively (Figure 4A). Similarly, a test with the SPC_3/SPC_2 ratio against the ApoB100 in LDL/ApoA1 in the HDL ratio (Figure 4B) shows a slightly lower correlation than that shown in Figure 4A ($r = 0.75$ and 0.85 , respectively, with $p = 2.2 \times 10^{-16}$ and 6.54×10^{-10} , respectively).

SPC Peak Linkage to LC–MS-Generated Serum Phospholipid Data (SHY-3). In the last level of SHY-*n*, the SPC integral regions were linked to LC–MS-generated quantitative lipidomic data (SHY-3, Figure 3D) obtained from the measurement of the same sample set. We focused only on the phospholipids with concentrations in the ¹H NMR

detection range to statistically link to the SPC signals, i.e., those likely to dominate the signal intensity. The means and standard deviations (Table S3) of the individual phospholipid concentrations for the control and SARS-CoV-2 patients (the latter printed in red) are shown in Figure 3D, while their statistical significance between infected and control groups is shown in Figures S3–S5. The majority of these phospholipids (9 out of 10 of those in the NMR detection range, Table S3) were significantly reduced in the SARS-CoV-2 patients, as previously reported.³⁸ Reduction in MS-measured phospholipids has been noted before in COVID-19 patients by others.⁶⁷ The pairwise statistical correlations of the individual phospholipids to the three SPC regions are shown in Figure 3D. The coefficients of determination sum to >1 because there is a degree of autocorrelation of the lipid components (they all decrease in SARS-CoV-2 infection to varying extents), as shown in the Supporting Data (targeted LC–MS lipid autocorrelation plots for control and COVID-19 patients in Figure S3). Nonetheless, these give estimates of which lipids contribute to the SPC components. All of the phospholipids included here contribute to the SPC_3 region in the control samples, and all of the phosphatidylcholines to SPC_1 and SPC_2 with a small contribution to SPC_2 variance from LPC 16:0 (Figure 3D).

In addition to changes in the phospholipid concentrations (Figure 3), we noted a change in the relationships of the SPC phospholipids between controls and SARS-CoV-2 patients. Specifically, lysophosphatidylcholine (LPC) 18:2 was increased in LDL (SPC_3) and HDL (SPC_2), whereas phosphatidylcholines, PC16:0/18:2, PC18:0/18:2, PC18:1/18:2, and PC18:2/18:2, were relatively reduced with weaker correlations to the SPC_2 and SPC_3 peaks. This is consistent with earlier observations on these lipid peaks in SARS-CoV-2 infection.⁶⁷ Increased activity of phospholipase A2 (PLA2)^{68,69} is directly

associated with the lipoprotein and is an independent marker of cardiovascular risk,⁷⁰ which can cleave a 16:0, 18:0, 18:1, or 18:2 fatty acid chain from each of the four PCs producing LPC 18:2.⁷¹ Given the known long-term clinical effects of SARS (SARS-CoV-1 virus) and persistence of symptoms in a high proportion of SARS survivors since 2003,⁶² it is important to note that COVID-19 exceeds the number of SARS cases by several orders of magnitude, and thus, PACS has the potential to overwhelm our health systems and economies. SARS persistent complications included chronic fatigue, hyperlipidemia, cardiovascular abnormality, and long-term increased rates of glycolysis linked to comprehensive elevations of plasma phosphatidylinositols and lysophosphatidylinositols.⁷² Therefore, any biomarker that has the potential to identify individuals at risk, thereby allowing earlier and more effective intervention is of critical value. In a recent large-scale statistical study (153,760 COVID-19 patients, 5,637,647 contemporary controls, and 5,859,411 historical controls) of COVID-19 outcomes at 1 year of disease onset, it was shown that the burden of cardiovascular disease is substantial.⁷³ This caused a variety of cardiac complications (inflammatory and ischemic heart disease, thrombotic disorders, heart failures, and dysrhythmia) even in nonseverely affected COVID-19 patients, resulting in an excess burden of more than 4% of all outcomes measured at the 12-month postacute phase. This potentially represents a staggering increase in cardiovascular risk worldwide given that over 400 million people have now contracted or are recovering from the disease. Thus, there is a critical need for identification of new, noninvasive markers of cardiovascular risk.

CONCLUSIONS

We have characterized the serum SPC NMR signal regions observed in healthy and SARS-CoV-2 positive patients with respect to lipoprotein subcompartments and lipidic speciation using a Statistical Heterospectroscopy in n -dimensions (SHY- n) approach. This enables molecular composition, compartmentation, and biological relationships of the SPC peaks to be established. In turn, this demonstrates the power of combined diffusion and relaxation spectroscopic methods with statistical spectroscopic methods for exploring compartmentally localized biomarkers of disease, where both concentration and molecular motion contribute to the diagnostic features of the biomarker. We detected strong correlations between the SPC peaks and NMR-generated apolipoprotein B100/A1 ratio, which itself is a well-established biomarker for cardiovascular, atherosclerosis, and myocardial infarction risk. We conclude that in addition to the diagnostic potential of the SPC signals in relation to COVID-19 diagnosis, they also carry important information about the structure and distributions of atherogenic plasma lipoproteins in the circulation. Thus, SPC NMR signals may provide information on long-term cardiovascular risks for COVID-19 patients and other patient subgroups.

ASSOCIATED CONTENT

Supporting Information

The Supporting Information is available free of charge at <https://pubs.acs.org/doi/10.1021/acs.analchem.1c05389>.

Cohort demographic data for the Spanish SARS-CoV-2 positive patients (Table S1); annotation of the keys used by the Bruker IVDr Lipoprotein Subclass Analysis method and mean \pm SD concentration of SARS-CoV-

2 positive and control samples (Table S2); annotation and the mean \pm SD concentration of lipids measured by ultrahigh-performance liquid chromatography–tandem mass spectrometry (UHPLC–MS/MS) that are used for the analysis (Table S3); group variance for both COVID-19-positive and control cohorts (Figure S1a); simulated 2D STOCSY maps of two broad and overlapped peaks A and B (Figure S1b); LC–MS phospholipids autocorrelation map (Figure S2); first- and fourth-dimension SHY (DIRE NMR to LC–MS phospholipids) (Figure S3); first- and second-dimension SHY (DIRE NMR to IVDr phospholipids) (Figure S4); and first- and third-dimension SHY (DIRE NMR to IVDr apolipoproteins) (Figure S5) (PDF)

AUTHOR INFORMATION

Corresponding Authors

Elaine Holmes – Australian National Phenome Center, and Center for Computational and Systems Medicine, Health Futures Institute, Murdoch University, Perth 6150 Western Australia, Australia; Department of Metabolism, Digestion and Reproduction, Faculty of Medicine, Imperial College London, London SW7 2AZ, U.K.; orcid.org/0000-0002-0556-8389; Email: elaine.holmes@murdoch.edu.au

Oscar Millet – Precision Medicine and Metabolism Laboratory, CIC bioGUNE, 48160 Derio, Spain; orcid.org/0000-0001-8748-4105; Email: omillet@cicbiogune.es

Julien Wist – Australian National Phenome Center, and Center for Computational and Systems Medicine, Health Futures Institute, Murdoch University, Perth 6150 Western Australia, Australia; Chemistry Department, Universidad del Valle, 76001 Cali, Colombia; orcid.org/0000-0002-3416-2572; Email: Julien.Wist@murdoch.edu.au, julien.wist@correounivalle.edu.co

Jeremy K. Nicholson – Australian National Phenome Center, and Center for Computational and Systems Medicine, Health Futures Institute, Murdoch University, Perth 6150 Western Australia, Australia; Department of Cardiology, Fiona Stanley Hospital, Medical School, University of Western Australia, Perth 6150 Western Australia, Australia; Institute of Global Health Innovation, Faculty of Medicine, Imperial College London, London SW7 2NA, U.K.; orcid.org/0000-0002-8123-8349; Email: Jeremy.Nicholson@murdoch.edu.au, j.nicholson@imperial.ac.uk

Authors

Reika Masuda – Australian National Phenome Center, and Center for Computational and Systems Medicine, Health Futures Institute, Murdoch University, Perth 6150 Western Australia, Australia

Samantha Lodge – Australian National Phenome Center, and Center for Computational and Systems Medicine, Health Futures Institute, Murdoch University, Perth 6150 Western Australia, Australia; orcid.org/0000-0001-9193-0462

Luke Whiley – Australian National Phenome Center, and Center for Computational and Systems Medicine, Health Futures Institute, Murdoch University, Perth 6150 Western Australia, Australia; orcid.org/0000-0002-9088-4799

Nicola Gray – Australian National Phenome Center, and Center for Computational and Systems Medicine, Health Futures Institute, Murdoch University, Perth 6150 Western Australia, Australia; orcid.org/0000-0002-0094-5245

Nathan Lawler – Australian National Phenome Center, and Center for Computational and Systems Medicine, Health Futures Institute, Murdoch University, Perth 6150 Western Australia, Australia; orcid.org/0000-0001-9649-425X

Philipp Nitschke – Australian National Phenome Center, and Center for Computational and Systems Medicine, Health Futures Institute, Murdoch University, Perth 6150 Western Australia, Australia

Sze-How Bong – Australian National Phenome Center, and Center for Computational and Systems Medicine, Health Futures Institute, Murdoch University, Perth 6150 Western Australia, Australia; orcid.org/0000-0002-3313-5097

Torben Kimhofer – Australian National Phenome Center, and Center for Computational and Systems Medicine, Health Futures Institute, Murdoch University, Perth 6150 Western Australia, Australia; orcid.org/0000-0001-7158-9930

Ruey Leng Loo – Australian National Phenome Center, and Center for Computational and Systems Medicine, Health Futures Institute, Murdoch University, Perth 6150 Western Australia, Australia; orcid.org/0000-0001-5307-5709

Berin Boughton – Australian National Phenome Center, and Center for Computational and Systems Medicine, Health Futures Institute, Murdoch University, Perth 6150 Western Australia, Australia; orcid.org/0000-0001-6342-9814

Annie X. Zeng – Australian National Phenome Center, and Center for Computational and Systems Medicine, Health Futures Institute, Murdoch University, Perth 6150 Western Australia, Australia

Drew Hall – Australian National Phenome Center, and Center for Computational and Systems Medicine, Health Futures Institute, Murdoch University, Perth 6150 Western Australia, Australia

Hartmut Schaefer – Bruker Biospin GmbH, Ettlingen 76275, Germany

Manfred Spraul – Bruker Biospin GmbH, Ettlingen 76275, Germany

Girish Dwivedi – Department of Cardiology, Fiona Stanley Hospital, Medical School, University of Western Australia, Perth 6150 Western Australia, Australia

Bu B. Yeap – Department of Endocrinology and Diabetes, Fiona Stanley Hospital, Medical School, University of Western Australia, Perth 6150 Western Australia, Australia

Tammo Diercks – Precision Medicine and Metabolism Laboratory, CIC bioGUNE, 48160 Derio, Spain

Ganeko Bernardo-Seisedos – Precision Medicine and Metabolism Laboratory, CIC bioGUNE, 48160 Derio, Spain

José M. Mato – Precision Medicine and Metabolism Laboratory, CIC bioGUNE, 48160 Derio, Spain

John C. Lindon – Department of Metabolism, Digestion and Reproduction, Faculty of Medicine, Imperial College London, London SW7 2AZ, U.K.; orcid.org/0000-0002-0916-6360

Complete contact information is available at:
<https://pubs.acs.org/10.1021/acs.analchem.1c05389>

Author Contributions

◆R.M. and S.L. contributed equally.

Notes

The authors declare no competing financial interest.

ACKNOWLEDGMENTS

The authors thank the Spinnaker Health Research Foundation, Western Australia; the McCusker Foundation, Western Australia; the Western Australian State Government (Premier's Intermediate Fellow funding for R.L.-L.); and the MRFF for funding the Australian National Phenome Centre for this and related work. They also thank MRFF Frontier Health and Medical Research (RFRHPI000147) grant to G.D., the Australian Research Council for Laureate Fellowship funding for E.H., and the NHMRC MRFF grant (2014349).

REFERENCES

- (1) Mokhtari, T.; Hassani, F.; Ghaffari, N.; Ebrahimi, B.; Yarahmadi, A.; Hassanzadeh, G. *J. Mol. Histol.* **2020**, *51*, 613–628.
- (2) Robba, C.; Battaglini, D.; Pelosi, P.; Rocco, P. R. M. *Expert Rev. Respir. Med.* **2020**, *14*, 865–868.
- (3) Nalbandian, A.; Sehgal, K.; Gupta, A.; Madhavan, M. V.; McGroder, C.; Stevens, J. S.; Cook, J. R.; Nordvig, A. S.; Shalev, D.; Sehrawat, T. S.; Ahluwalia, N.; Bikdeli, B.; Dietz, D.; Der-Nigoghossian, C.; Liyanage-Don, N.; Rosner, G. F.; Bernstein, E. J.; Mohan, S.; Beckley, A. A.; Seres, D. S.; Choueiri, T. K.; Uriel, N.; Ausiello, J. C.; Accili, D.; Freedberg, D. E.; Baldwin, M.; Schwartz, A.; Brodie, D.; Garcia, C. K.; Elkind, M. S. V.; Connors, J. M.; Bilezikian, J. P.; Landry, D. W.; Wan, E. Y. *Nat. Med.* **2021**, *27*, 601–615.
- (4) Peluso, M. J.; Lu, S.; Tang, A. F.; Durstenfeld, M. S.; Ho, H.-E.; Goldberg, S. A.; Forman, C. A.; Munter, S. E.; Hoh, R.; Tai, V.; Chenna, A.; Yee, B. C.; Winslow, J. W.; Petropoulos, C. J.; Greenhouse, B.; Hunt, P. W.; Hsue, P. Y.; Martin, J. N.; Daniel Kelly, J.; Glidden, D. V.; Deeks, S. G.; Henrich, T. J. *J. Infect. Dis.* **2021**, *224*, 1839–1848.
- (5) Holmes, E.; Wist, J.; Masuda, R.; Lodge, S.; Nitschke, P.; Kimhofer, T.; Loo, R. L.; Begum, S.; Boughton, B.; Yang, R.; Morillon, A.-C.; Chin, S.-T.; Hall, D.; Ryan, M.; Bong, S.-H.; Gay, M.; Edgar, D. W.; Lindon, J. C.; Richards, T.; Yeap, B. B.; Pettersson, S.; Spraul, M.; Schaefer, H.; Lawler, N. G.; Gray, N.; Whiley, L.; Nicholson, J. K. *J. Proteome Res.* **2021**, *20*, 3315–3329.
- (6) Nicholson, J. K. *Phenomics* **2021**, *1*, 143–150.
- (7) Zheng, Y. Y.; Ma, Y. T.; Zhang, J. Y.; Xie, X. *Nat. Rev. Cardiol.* **2020**, *17*, 259–260.
- (8) Solomon, T. *Nat. Rev. Neurol.* **2021**, *17*, 65–66.
- (9) Nicholson, J. K.; Wilson, I. D. *Prog. Nucl. Magn. Reson. Spectrosc.* **1989**, *21*, 449–501.
- (10) Nicholson, J. K.; Buckingham, M. J.; Sadler, P. J. *Biochem. J.* **1983**, *211*, 605–615.
- (11) Bell, J. D.; Sadler, P. J.; Macleod, A. F.; Turner, P. R.; La Ville, A. *FEBS Lett.* **1987**, *219*, 239–243.
- (12) Nicholson, J. K.; O'Flynn, M. P.; Sadler, P. J.; Macleod, A. F.; Juul, S. M.; Sonksen, P. H. *Biochem. J.* **1984**, *217*, 365–375.
- (13) Nicholson, J. K.; Foxall, P. J.; Spraul, M.; Farrant, R. D.; Lindon, J. C. *Anal. Chem.* **1995**, *67*, 793–811.
- (14) Beckonert, O.; Keun, H. C.; Ebbels, T. M.; Bundy, J.; Holmes, E.; Lindon, J. C.; Nicholson, J. K. *Nat. Protoc.* **2007**, *2*, 2692–2703.
- (15) Nicholson, J. K.; Lindon, J. C.; Holmes, E. *Xenobiotica* **1999**, *29*, 1181–1189.
- (16) Otvos, J. D.; Shalauova, I.; Wolak-Dinsmore, J.; Connelly, M. A.; Mackey, R. H.; Stein, J. H.; Tracy, R. P. *Clin. Chem.* **2015**, *61*, 714–723.
- (17) Bell, J. D.; Brown, J. C. C.; Nicholson, J. K.; Sadler, P. J. *FEBS Lett.* **1987**, *215*, 311–315.
- (18) Otvos, J. D.; Jeyarajah, E. J.; Bennett, D. W. *Clin. Chem.* **1991**, *37*, 377–386.
- (19) Ala-Korpela, M.; Korhonen, A.; Keisala, J.; Hörkö, S.; Korpi, P.; Ingman, L. P.; Jokisaari, J.; Savolainen, M. J.; Kesäniemi, Y. A. *J. Lipid Res.* **1994**, *35*, 2292–2304.
- (20) Dona, A. C.; Jimenez, B.; Schafer, H.; Humpfer, E.; Spraul, M.; Lewis, M. R.; Pearce, J. T.; Holmes, E.; Lindon, J. C.; Nicholson, J. K. *Anal. Chem.* **2014**, *86*, 9887–9894.

- (21) Carr, H. Y.; Purcell, E. M. *Phys. Rev.* **1954**, *94*, 630–638.
- (22) Stejskal, E. O.; Tanner, J. E. *J. Chem. Phys.* **1965**, *42*, 288–292.
- (23) Stejskal, E. O. *J. Chem. Phys.* **1965**, *43*, 3597–3603.
- (24) Wu, D.; Chen, A.; Johnson, S. C., Jr. *J. Magn. Reson. A* **1996**, *123*, 215–218.
- (25) Jerschow, A.; Müller, N. *J. Magn. Reson. A* **1996**, *123*, 222–225.
- (26) Liu, M.; Nicholson, J. K.; Parkinson, J. A.; Lindon, J. C. *Anal. Chem.* **1997**, *69*, 1504–1509.
- (27) Liu, M.; Nicholson, J. K.; Lindon, J. C. *Anal. Chem.* **1996**, *68*, 3370–3376.
- (28) Lodge, S.; Nitschke, P.; Kimhofer, T.; Wist, J.; Bong, S.-H.; Loo, R. L.; Masuda, R.; Begum, S.; Richards, T.; Lindon, J. C.; Bermel, W.; Reinsperger, T.; Schaefer, H.; Spraul, M.; Holmes, E.; Nicholson, J. K. *Anal. Chem.* **2021**, *93*, 3976–3986.
- (29) Bizkarguenaga, M.; Bruzzone, C.; Gil-Redondo, R.; SanJuan, I.; Martin-Ruiz, I.; Barriales, D.; Palacios, A.; Pasco, S. T.; González-Valle, B.; Lain, A.; Herrera, L.; Azkarate, A.; Vesga, M. A.; Eguizabal, C.; Anguita, J.; Embade, N.; Mato, J. M.; Millet, O. *NMR Biomed.* **2021**, No. e4637.
- (30) Schmelter, F.; Foeh, B.; Mallagaray, A.; Rahmoeller, J.; Ehlers, M.; Lehrian, S.; von Kopylow, V.; Künsting, I.; Lixenfeld, A. S.; Martin, E.; Ragab, M.; Borsche, M.; Balck, A.; Vollstedt, E. J.; Meyer-Saraei, R.; Kreutzmann, F.; Eitel, I.; Taube, S.; Klein, C.; Katalinic, A.; Rupp, J.; Jantzen, E.; Graf, T.; Sina, C.; Günther, U. L. Metabolic Markers Distinguish COVID-19 from Other Intensive Care Patients and Show Potential to Stratify for Disease Risk *medRxiv* 2021, 7, DOI: 10.1101/2021.01.13.21249645.
- (31) Hilsner, J. R.; Han, Y.; Biswas, S.; Gukasyan, J.; Cai, Z.; Zhu, R.; Tang, W. H. W.; Deb, A.; Lusic, A. J.; Hartiala, J. A.; Allayee, H. *J. Lipid Res.* **2021**, *62*, No. 100061.
- (32) Begue, F.; Tanaka, S.; Mouktadi, Z.; Rondeau, P.; Veeren, B.; Diotel, N.; Tran-Dinh, A.; Robert, T.; Vélia, E.; Mavingui, P.; Lagrange-Xélot, M.; Montravers, P.; Couret, D.; Meilhac, O. *Sci. Rep.* **2021**, *11*, No. 2291.
- (33) Garcia-Perez, I.; Poma, J. M.; Serrano-Contreras, J. I.; Boulangé, C. L.; Chan, Q.; Frost, G.; Stamler, J.; Elliott, P.; Lindon, J. C.; Holmes, E.; Nicholson, J. K. *Nat. Protoc.* **2020**, *15*, 2538–2567.
- (34) Cloarec, O.; Dumas, M. E.; Craig, A.; Barton, R. H.; Trygg, J.; Hudson, J.; Blancher, C.; Gauguier, D.; Lindon, J. C.; Holmes, E.; Nicholson, J. *Anal. Chem.* **2005**, *77*, 1282–1289.
- (35) Crockford, D. J.; Holmes, E.; Lindon, J. C.; Plumb, R. S.; Zirah, S.; Bruce, S. J.; Rainville, P.; Stumpf, C. L.; Nicholson, J. K. *Anal. Chem.* **2006**, *78*, 363–371.
- (36) Blaise, B. J.; Correia, G. D. S.; Haggart, G. A.; Surowiec, I.; Sands, C.; Lewis, M. R.; Pearce, J. T. M.; Trygg, J.; Nicholson, J. K.; Holmes, E.; Ebbels, T. M. D. *Nat. Protoc.* **2021**, *16*, 4299–4326.
- (37) Baumstark, D.; Kremer, W.; Boettcher, A.; Schreier, C.; Sander, P.; Schmitz, G.; Kirchhoefer, R.; Huber, F.; Kalbitzer, H. R. *J. Lipid Res.* **2019**, *60*, 1516–1534.
- (38) Gray, N.; Lawler, N. G.; Zeng, A. X.; Ryan, M.; Bong, S. H.; Boughton, B. A.; Bizkarguenaga, M.; Bruzzone, C.; Embade, N.; Wist, J.; Holmes, E.; Millet, O.; Nicholson, J. K.; Whiley, L. *Metabolites* **2021**, *11*, No. 467.
- (39) Jiménez, B.; Holmes, E.; Heude, C.; Tolson, R. F.; Harvey, N.; Lodge, S. L.; Chetwynd, A. J.; Cannet, C.; Fang, F.; Pearce, J. T. M.; Lewis, M. R.; Viant, M. R.; Lindon, J. C.; Spraul, M.; Schaefer, H.; Nicholson, J. K. *Anal. Chem.* **2018**, *90*, 11962–11971.
- (40) Loo, R. L.; Lodge, S.; Kimhofer, T.; Bong, S. H.; Begum, S.; Whiley, L.; Gray, N.; Lindon, J. C.; Nitschke, P.; Lawler, N. G.; Schaefer, H.; Spraul, M.; Richards, T.; Nicholson, J. K.; Holmes, E. *J. Proteome Res.* **2020**, *19*, 4428–4441.
- (41) Adams, K. J.; Pratt, B.; Bose, N.; Dubois, L. G.; St John-Williams, L.; Perrott, K. M.; Ky, K.; Kapahi, P.; Sharma, V.; MacCoss, M. J.; Moseley, M. A.; Colton, C. A.; MacLean, B. X.; Schilling, B.; Thompson, J. W. *J. Proteome Res.* **2020**, *19*, 1447–1458.
- (42) Luan, H.; Ji, F.; Chen, Y.; Cai, Z. *Anal. Chim. Acta* **2018**, *1036*, 66–72.
- (43) Murphy, H. C.; Ala-Korpela, M.; White, J. J.; Raouf, A.; Bell, J. D.; Barnard, M. L.; Burns, S. P.; Iles, R. A. *Biochem. Biophys. Res. Commun.* **1997**, *234*, 733–737.
- (44) Murphy, H. C.; Burns, S. P.; White, J. J.; Bell, J. D.; Iles, R. A. *Biochemistry* **2000**, *39*, 9763–9770.
- (45) Ala-Korpela, M.; Lankinen, N.; Salminen, A.; Suna, T.; Soininen, P.; Laatikainen, R.; Ingman, P.; Jauhiainen, M.; Taskinen, M.-R.; Héberger, K.; Kaski, K. *Atherosclerosis* **2007**, *190*, 352–358.
- (46) Masana, L.; Correig, E.; Ibarretxe, D.; Anoro, E.; Arroyo, J. A.; Jericó, C.; Guerrero, C.; la Miret, M.; Näf, S.; Pardo, A.; Perea, V.; Pérez-Bernalte, R.; Plana, N.; Ramírez-Montesinos, R.; Royuela, M.; Soler, C.; Urquiza-Padilla, M.; Zamora, A.; Pedro-Botet, J.; STACOV-XULA research group. *Sci. Rep.* **2021**, *11*, No. 7217.
- (47) Masuda, R.; Lodge, S.; Nitschke, P.; Spraul, M.; Schaefer, H.; Bong, S.-H.; Kimhofer, T.; Hall, D.; Loo, R. L.; Bizkarguenaga, M.; Bruzzone, C.; Gil-Redondo, R.; Embade, N.; Mato, J. M.; Holmes, E.; Wist, J.; Millet, O.; Nicholson, J. K. *J. Proteome Res.* **2021**, *20*, 4139–4152.
- (48) Jacob, G.; Aharon, A.; Brenner, B. *Front. Physiol.* **2020**, *11*, No. 596057.
- (49) Mast, A. E.; Wolberg, A. S.; Gailani, D.; Garvin, M. R.; Alvarez, C.; Miller, J. I.; Aronow, B.; Jacobson, D. *eLife* **2021**, *10*, No. e64330.
- (50) Merrill, J. T.; Erkan, D.; Winakur, J.; James, J. A. *Nat. Rev. Rheumatol.* **2020**, *16*, 581–589.
- (51) Yin, S.; Huang, M.; Li, D.; Tang, N. *J. Thromb. Thrombolysis* **2021**, *51*, 1107–1110.
- (52) Milne, R. W.; Marcel, Y. L. *FEBS Lett.* **1982**, *146*, 97–100.
- (53) Elovson, J.; Chatterton, J. E.; Bell, G. T.; Schumaker, V. N.; Reuben, M. A.; Puppione, D. L.; Reeve, J. R., Jr.; Young, N. L. *J. Lipid Res.* **1988**, *29*, 1461–1473.
- (54) Walldius, G. The apoB/apoA-I Ratio Is a Strong Predictor of Cardiovascular Risk. In *Lipoproteins*; Frank, S.; Kostner, G., Eds.; IntechOpen: Rijeka, 2012.
- (55) Panayiotou, A.; Griffin, M.; Georgiou, N.; Bond, D.; Tyllis, T.; Tziakouri-Shiakalli, C.; Fessas, C.; Nicolaides, A. *Int. Angiol.* **2008**, *27*, 74–80.
- (56) Ljungberg, J.; Holmgren, A.; Bergdahl, I. A.; Hultdin, J.; Norberg, M.; Näslund, U.; Johansson, B.; Söderberg, S. *J. Am. Heart Assoc.* **2017**, *6*, No. e007160.
- (57) Bodde, M. C.; Hermans, M. P. J.; Jukema, J. W.; Schali, M. J.; Lijfering, W. M.; Rosendaal, F. R.; Romijn, F. P. H. T. M.; Ruhaak, L. R.; van der Laarse, A.; Cobbaert, C. M. *Clin. Res. Cardiol.* **2019**, *108*, 520–538.
- (58) Kaneva, A. M.; Potolitsyna, N. N.; Bojko, E. R.; Odland, JØ. *Dis. Markers* **2015**, *2015*, No. 591454.
- (59) Bae, S.; Kim, S. R.; Kim, M.-N.; Shim, W. J.; Park, S.-M. *Heart* **2021**, *107*, 373–380.
- (60) Nishiga, M.; Wang, D. W.; Han, Y.; Lewis, D. B.; Wu, J. C. *Nat. Rev. Cardiol.* **2020**, *17*, 543–558.
- (61) Zaman, S.; MacIsaac, A. I.; Jennings, G. L.; Schlaich, M. P.; Inglis, S. C.; Arnold, R.; Kumar, S.; Thomas, L.; Wahi, S.; Lo, S.; Naismith, C.; Duffy, S. J.; Nicholls, S. J.; Newcomb, A.; Almeida, A. A.; Wong, S.; Lund, M.; Chew, D. P.; Kritharides, L.; Chow, C. K.; Bhindi, R. *Med. J. Aust.* **2020**, *213*, 182–187.
- (62) Oudit, G. Y.; Kassiri, Z.; Jiang, C.; Liu, P. P.; Poutanen, S. M.; Penninger, J. M.; Butany, J. *Eur. J. Clin. Invest.* **2009**, *39*, 618–625.
- (63) Cavalieri, C.; Rohrer, L.; von Eckardstein, A. *Circ. Res.* **2006**, *99*, 1060–1066.
- (64) Zhu, Z.; Yang, Y.; Fan, L.; Ye, S.; Lou, K.; Hua, X.; Huang, Z.; Shi, Q.; Gao, G. *J. Clin. Lab. Anal.* **2021**, *35*, No. e23911.
- (65) Walldius, G.; Jungner, I.; Holme, I.; Aastveit, A. H.; Kolar, W.; Steiner, E. *Lancet* **2001**, *358*, 2026–2033.
- (66) Yusuf, S.; Hawken, S.; Ounpuu, S.; Dans, T.; Avezum, A.; Lanas, F.; McQueen, M.; Budaj, A.; Pais, P.; Varigos, J.; Lisheng, L.; INTERHEART Study Investigators. *Lancet* **2004**, *364*, 937–952.
- (67) Cai, Y.; Kim, D. J.; Takahashi, T.; Broadhurst, D. I.; Yan, H.; Ma, S.; Rattray, N. J. W.; Casanovas-Massana, A.; Israelow, B.; Klein, J.; Lucas, C.; Mao, T.; Moore, A. J.; Muenker, M. C.; Oh, J. E.; Silva, J.; Wong, P.; Yale IMPACT Research team; Ko, A. I.; Khan, S. A.;

Iwasaki, A.; Johnson, C. H. Kynurenic Acid May Underlie Sex-Specific Immune Responses to COVID-19. *Sci. Signal.* **2021**, *14* (). eabf8483. DOI: 10.1126/scisignal.abf8483.

(68) Snider, J. M.; You, J. K.; Wang, X.; Snider, A. J.; Hallmark, B.; Zec, M. M.; Seeds, M. C.; Sergeant, S.; Johnstone, L.; Wang, Q.; Sprissler, R.; Carr, T. F.; Lutrick, K.; Parthasarathy, S.; Bime, C.; Zhang, H. H.; Luberto, C.; Kew, R. R.; Hannun, Y. A.; Guerra, S.; McCall, C. E.; Yao, G.; Del Poeta, M.; Chilton, F. H. *J. Clin. Invest.* **2021**, *131*, No. e149236.

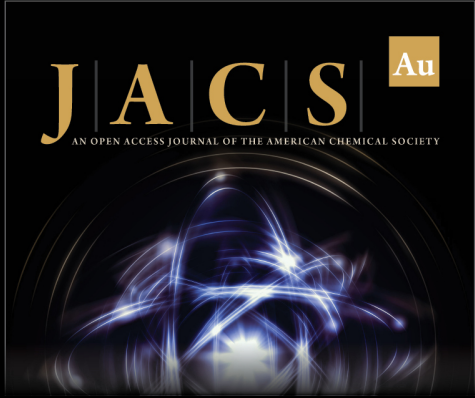
(69) Kuypers, F. A.; Rostad, C. A.; Anderson, E. J.; Chahroudi, A.; Jaggi, P.; Wrammert, J.; Mantus, G.; Basu, R.; Harris, F.; Hanberry, B.; Camacho-Gonzalez, A.; Manoranjithan, S.; Vos, M.; Brown, L. A.; Morris, C. R. *Exp. Biol. Med.* **2021**, *246*, 2543–2552.

(70) Packard, C. J.; O'Reilly, D. S.; Caslake, M. J.; McMahon, A. D.; Ford, I.; Cooney, J.; Macphee, C. H.; Suckling, K. E.; Krishna, M.; Wilkinson, F. E.; Rumley, A.; Lowe, G. D.; et al. *N. Engl. J. Med.* **2000**, *343*, 1148–1155.


(71) Barberis, E.; Timo, S.; Amede, E.; Vanella, V. V.; Puricelli, C.; Cappellano, G.; Raineri, D.; Cittone, M. G.; Rizzi, E.; Pedrinelli, A. R.; Vassia, V.; Casciaro, F. G.; Priora, S.; Nerici, I.; Galbiati, A.; Hayden, E.; Falasca, M.; Vaschetto, R.; Sainaghi, P. P.; Dianzani, U.; Rolla, R.; Chiocchetti, A.; Baldanzi, G.; Marengo, E.; Manfredi, M. *Int. J. Mol. Sci.* **2020**, *21*, No. 8623.


(72) Wu, Q.; Zhou, L.; Sun, X.; Yan, Z.; Hu, C.; Wu, J.; Xu, L.; Li, X.; Liu, H.; Yin, P.; Li, K.; Zhao, J.; Li, Y.; Wang, X.; Li, Y.; Zhang, Q.; Xu, G.; Chen, H. *Sci. Rep.* **2017**, *7*, No. 9110.


(73) Xie, Y.; Xu, E.; Bowe, B.; Al-Aly, Z. *Nat. Med.* **2022**, 1–8.



JACS Au
AN OPEN ACCESS JOURNAL OF THE AMERICAN CHEMICAL SOCIETY

 Editor-in-Chief
Prof. Christopher W. Jones
Georgia Institute of Technology, USA

Open for Submissions 

pubs.acs.org/jacsau  ACS Publications
Most Trusted. Most Cited. Most Read.